Volume 1 | Number 1 | Jan 2013 | Pages 1–100

Journal of
Materials Chemistry A

Materials for energy and sustainability
www.rsc.org/materialsA

Li⁺

ROYAL SOCIETY
OF CHEMISTRY

ROYAL SOCIETY
OF CHEMISTRY

www.rsc.org/materialsA

Table of Content (TOC)

A soluble conducting polymer composite with graphene oxide showed tunable actuation behavior under different voltages.

ARTICLE TYPE

Soluble Conducting Polymer-Functionalized Graphene Oxide for Air-Operable Actuator Fabrication

Madeshwaran Sekkarapatti Ramasamy,[a] Sibdas Singha Mahapatra,[a] Hye Jin Yoo,[a] Yoong Ahm Kim,[b] Jae Whan Cho[a]*

An effective route for the preparation of a processable, conducting polymer-functionalized graphene oxide for actuator applications is investigated. First, graphene oxide (GO) is covalently functionalized with a 3-thiophene acetic acid (TAA) monomer by esterification. Then, the TAA-functionalized GO is self-polymerized by chemical oxidative polymerization to yield poly(3-thiophene acetic acid)-functionalized GO (GO-f-PTAA). Further, the GO-f-PTAA is also copolymerized with thiophene (Th) to yield GO-f-PTAA-co-PTh. The synthesis of GO-f-PTAA and GO-f-PTAA-co-PTh composites is confirmed by Fourier transform infrared, [1]H-nuclear magnetic resonance, and X-ray photoelectron spectroscopies. The composites show better electrochemical properties than pure PTAA and superior solubility in organic solvents compared to pure GO. Using the soluble GO-f-PTAA and GO-f-PTAA-co-PTh composites, air-operable actuators are fabricated and their actuation performance is investigated. The copolymer-functionalized GO actuator exhibits good
15 electroactive actuation behavior between 2 and 4 V, mainly because of the enhanced electrochemical performance of the composites, whereas the pure PTAA and GO-f-PTAA actuators do not show actuation under the applied voltage. The soluble conducting polymer-functionalized graphene composites developed in this study have potential applications in the fabrication of actuators that can be operated in air.

1 Introduction

20 Electroactive polymers (EAPs) have received a great deal of attention in the last decade for their potential applications in biomimetic actuators, robots, and microelectromechanical systems.[1] These polymers have many attractive features such as a
25 low weight, low cost, flexibility, and the ability to undergo large deformation, especially as compared to conventional electromechanical ceramics and shape-memory alloys. Various types of EAPs, including dielectric elastomers, piezoelectric polymers, electrostrictives, ionic polymer metal composites, and
30 conducting polymers, have been extensively researched.[2-6] Of these materials, the conducting polymers are more attractive as actuator materials owing to their low voltage requirement for actuation, high strength, and large strain tolerance. However, the drawbacks of the existing state-of-the-art conducting polymers
35 include their poor processability, which often makes actuator fabrication difficult.

   Among the various types of conducting polymers, polythiophenes are well known for their potential applications in photovoltaic devices and field-effect transistors.[7,8]
40 Polythiophenes with long and flexible side chains at the third position of the thiophene ring were found to be soluble in some organic solvents.[9] In particular, the use of poly(3-thiophene acetic acid) (PTAA) with -COOH functional groups not only improves the processability of the polymer but also offers the utility of -
45 COOH groups for further functionalization.[10] However, the electrical conductivity of PTAA is very low. For example,

Mukherjee et al. reported a conductivity value of 1.02×10^{-8} S/cm for pure PTAA synthesized by chemical oxidative polymerization, which is low for practical applications.[11]
50 Recently, nanocarbon materials such as carbon nanotubes and graphene, which have excellent electrical and mechanical properties with large surface areas, have emerged as potential candidates for applications in actuators, transistors, and photovoltaic devices.[12-17] The incorporation of nanocarbon
55 materials as the filler in polymer nanocomposites could substantially enhance the crucial properties of the composites, offering an appropriate actuator material with the desired properties. Accordingly, a few researchers have already investigated nanocomposite-based actuators synthesized using the
60 solution mixing method with graphene or graphene oxide (GO) as a nanofiller.[18,19] Until now, the covalent functionalization approach, which is more effective for achieving effective dispersion of graphene in a polymer matrix, has been almost unexplored for actuator fabrication.

65   In order to develop soluble conducting polymers grafted to GO for use in high-performance dry-type actuators, we have explored processable thiophene-based GO composites produced using the covalent functionalization method. The soluble conducting polymer-functionalized GO in this study can afford high
70 processability as well as good dispersion and enhanced electrical properties due to the covalent bonding of conducting polymer and GO. Using the soluble composites, we have fabricated air-operable actuators with the polymer electrolyte as the electrolyte layer. The electro-chemomechanical properties as well as the
75 structural features, thermal properties, and processability of

soluble conducting composites were investigated in this study.

2 Experimental

Materials

GO was received from Nanoinnovo Technologies (Madrid, Spain), and 3-thiopheneacetic acid (TAA), *N,N'*-dicyclohexylcarbodiimide (DCC), 4-dimetylaminopyridine (DMAP), poly(vinylidene fluoride) (PVDF), bis(trifluoromethane)sulfonamide lithium salt (LiTFSi), and *N,N'*-dimethylformamide (DMF) were purchased from Sigma Aldrich, Korea. Ferric chloride was obtained from Samchun chemicals, Korea. Tetrahydrofuran (THF), methanol, and chloroform were purchased from SK chemicals, Korea.

Covalent functionalization of graphene oxide with 3-thiophene acetic acid monomer

First, 200 mg of GO in 10 mL of DMF was sonicated with a bath-type sonicator for 40 min to produce a homogeneous suspension of GO. Then, 1 g of TAA (7.0333 mmol) in 5 mL DMF was added to the GO suspension and stirred for further 30 min. A solution of DCC (1.4511 g, 7.0333 mmol) and DMAP (0.0855 g, 0.700 mmol) in 4 mL of DMF was then charged into the GO/TAA suspension, and the reaction mixture was stirred for 4 days under a nitrogen atmosphere at room temperature. After the completion of the esterification reaction, DMF was removed by filtration, and the resultant monomer-functionalized GO (GO-f-TAA) was washed with plenty of DMF and methanol and dried at 40 °C under vacuum.[20]

Synthesis of poly(3-thiophene acetic acid)-functionalized GO (GO-f-PTAA)

First, 100 mg of GO-f-TAA was sonicated in a 10 mL of dry chloroform for 30 min to produce a GO-f-TAA suspension. Then, 40 mg of ferric chloride in 10 mL of chloroform was added the to GO-f-TAA suspension, and the reaction mixture was stirred at room temperature for 24 h to complete the chemical oxidative polymerization process. Excess chloroform was added to the reaction mixture, and the GO-f-PTAA was obtained after vacuum filtration and drying at 40 °C under vacuum.

Synthesis of copolymer-functionalized GO (GO-f-PTAA-co-PTh)

First, 100 mg of GO-f-TAA was added to 10 mL of chloroform and sonicated for 30 min. To the resultant suspension, 40 mg of ferric chloride in 10 mL of chloroform was added. Then, 1.2 mL of thiophene (Th) was slowly injected to the reaction mixture and stirred for 24 h at room temperature under a nitrogen atmosphere. The reaction mixture was filtered, and the residue was dried at 40 °C to obtain GO-f-PTAA-co-PTh. In addition, for comparative studies, pure PTAA was synthesized by chemical oxidative polymerization following the reported procedures.[21] Briefly, 20 mmol of anhydrous ferric chloride was dissolved in 15 mL of chloroform in a three-necked flask under a nitrogen atmosphere. Then, 5 mmol of the TAA monomer in 10 mL of chloroform solution was added slowly and stirred for 24 h at room temperature. The reaction mixture was filtered, washed with methanol, and then dried under vacuum to yield PTAA.

Fabrication of air-operable conducting polymer actuator

The actuator samples were composed of several layers: an Al bottom electrode/active layer/solid polymer electrolyte (SPE)/active layer/Al top electrode structure was prepared on a polyimide (PI) substrate cleaned in methanol and distilled water in an ultrasonic bath for 15 min (Fig. S1). Note that the active layer is GO-f-PTAA or GO-f-PTAA-co-PTh, and SPE represents the PVDF-LiTFSi electrolyte. Briefly, Al bottom electrodes with a thickness of 50 nm were thermally evaporated on the PI under a vacuum of 10^{-6} Torr at 1 Å/s with a patterned shadow mask. The active layer dispersed in DMF solution was spin-coated on the PI substrate at 1500 rpm for 60 sec, after which the SPE layer was spin-coated with different concentrations of LiTFSi (0.025 M, 0.05 M, 0.1 M) using 10 wt% PVDF solution in DMF and dried under vacuum at 50 °C to remove the DMF. Then active layer was once again spin-coated on the SPE layer to complete the trilayer actuator configuration. Al top electrode lines with thicknesses of 50 nm were then finally deposited on the active layer by thermal evaporation with a deposition rate of 1 Å/s at a pressure of 10^{-6} Torr. The top electrode lines were aligned perpendicular to the bottom electrode lines to form 4×4 arrays of actuator cells with an active area of 5×5 mm^2.

Characterization

Fourier transform infrared spectroscopic (FT-IR) studies were performed using a Jasco FT-IR 300E apparatus (Tokyo, Japan) with KBr as a standard. For SEM (FE-SEM, S-4300SE, Hitachi) measurements, the samples were prepared by spin-coating the nanocomposite solution (0.5 mg/mL in DMF) on a silicon wafer at 2000 rpm for 60 sec. High-resolution transmission electron microscopy (HR-TEM) images of the samples dispersed in THF solution and then dropped on 400 mesh copper grids with supporting carbon films were obtained using a JEM 2100 instrument (JEOL). The nanostructures of spin coated samples (2000 rpm for 60 seconds) on silicon wafers were observed using tapping-mode atomic force microscopy (TM-AFM, Nanoscope IV Digital Instruments). The surface chemical composition of the GO and GO-f-TAA samples was measured by performing X-ray photoelectron spectroscopy (XPS, ESCSA 2000). The electrical conductivity of the samples was measured by a four-probe conductivity measurement apparatus (Jandel, Model RM3-AR) at room temperature. The thermogravimetric analysis of the samples was carried out using a TA Q50 thermal analyzer at a heating rate of 5 °C min^{-1} under a nitrogen atmosphere. The proton nuclear magnetic resonance (^{1}H-NMR) spectra were recorded by a 600 MHz NMR spectrometer with dimethyl sulfoxide-d$_6$ as a solvent and tetramethylsilane as an internal standard. Cyclic voltammetry measurements were carried out using a three-electrode cell system (working electrode, counter electrode, and reference electrode) in order to study the electrochemical behaviour of the samples. Ag/AgCl, platinum sheet, and glassy carbon were used as the reference electrode, counter electrode, and working electrode, respectively. The working electrode was prepared by dropping and drying a

solution of the sample on a glassy carbon electrode. The electrolyte used in this study was 1 M sulphuric acid. All electrochemical measurements were carried out in a potential window from -0.2 V to 0.8 V with different scan rates (10 mV/s, 5 20 mV/s, 50 mV/s, and 100 mV/s).

3 Results and Discussion

The synthesis of GO-f-PTAA and GO-f-PTAA-co-PTh was carried out in two steps, as shown in Scheme 1. In the first step, the monomer was grafted with GO by the esterification reaction, 10 and followed by homopolymerization or copolymerization in the second step to yield the GO-f-PTAA or GO-f-PTAA-co-PTh composites, respectively. The synthesized composites were easily dispersed in solvents such as DMF and THF, facilitating spin coating for the device fabrication. The good dispersion of 15 composites in the solvent could be confirmed by linear absorbance at 500 nm with concentration of solution in the UV/Vis measurements (Fig. S2).
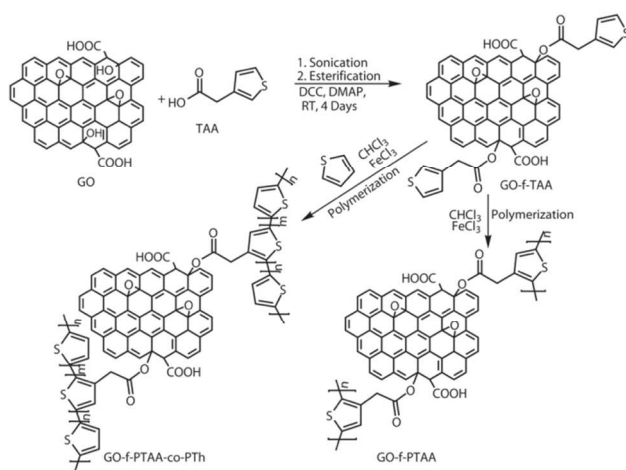

Scheme 1 Schematic illustration of covalent functionalization of 20 3-thiophene acetic acid monomer with GO by esterification reaction, followed by oxidative polymerization to produce GO-f-PTAA and GO-f-PTAA-CO-PTh composites.

Figs. 1a and 1b show the XPS results for GO and GO-f-TAA, respectively. The XPS spectrum of GO shows only carbon and 25 oxygen peaks, whereas the XPS spectrum of the GO-f-TAA shows carbon, oxygen, and sulfur peaks attributable to both GO and TAA, revealing the success of the esterification reaction. Fig. 1c displays the high-resolution C 1s XPS spectra of GO, where the signals of C-C, C-O, and C=O groups at 284.599, 286.415, 30 and 288.336 eV, respectively, confirm that the GO contains oxygen-containing groups such as epoxy, hydroxyl, and carbonyl groups.[22] After the TAA monomer is grafted on the GO, the intensities of C-C and C=O groups were increased (Fig. 1d) because of the carbons and carbonyl groups in the thiophene rings 35 of the TAA. Meanwhile, the intensity of the C-O groups was decreased after the monomer grafting, which suggests the possible activation of hydroxyl groups by DCC and DMAP and subsequent attachment of the monomer to GO. In the GO-f-TAA spectra, the presence of ester bonds was also confirmed by the 40 peaks at 286.46 and 288.073 eV, corresponding to C-O and C=O groups, respectively.[23]

The functional groups of GO, GO-f-TAA, GO-f-PTAA, and GO-f-PTAA-co-PTh were analyzed by performing FT-IR spectroscopy (Fig. 2a). The GO shows the characteristic peaks at 45 3418, 1738, 1227, 1058, and 1648 cm^{-1} due to the hydroxyl (O-H) group, carboxylic acid (C=O) group, C-OH group, C-O group, and C-C skeletal vibration of GO, respectively. The presence of ester linkages in GO-f-TAA was confirmed by the observation of peaks at 1740 and 1251 cm^{-1}, which are attributed to the C=O and 50 C-O groups of the ester bond. In addition, a new peak was observed around 1097 cm^{-1} for GO-f-TAA, which was assigned to the C-S stretching vibration of the thiophene ring.[24] The presence of ester and C-S stretching vibration peaks confirms the success of monomer (TAA) grafting with GO. In addition to the 55 ester peaks, the FT-IR spectra of GO-f-PTAA and GO-f-PTAA-co-PTh show C-S stretching vibrations of the thiophene rings at around 1113, 980, and 750 cm^{-1}, confirming that both the homopolymer and copolymer were covalently grafted with GO. The Raman spectra were also used to characterize the structural 60 changes occurring during the functionalization of GO with the conducting polymers (Fig. 2b). The GO exhibits the G-band at 1590 cm^{-1} (E_{2g2} graphite mode) along with the D-band (the defect-induced mode) at 1349 cm^{-1}.[25] The I_D/I_G (the integrated intensity of the D band divided by the integrated intensity of the 65 G band) indicates the extent of disorder present in the graphene sheets. In our case, the I_D/I_G values of GO, GO-f-TAA, GO-f-PTAA, and GO-f-PTAA-co-PTh were found to be 0.92, 0.99, 1.00, and 0.99, respectively, indicating that the extent of disorder in the samples are similar. This is because the covalent 70 functionalization was achieved by using the hydroxyl groups of GO, so the skeletal structure of GO was well preserved during the functionalization.[26] The functionalization and polymerization of GO-f-TAA, GO-f-PTAA, and GO-f-PTAA-co-PTh were further confirmed by ^{1}H-NMR spectroscopy. The spectra of the TAA-75 functionalized GO and its polymers were in good agreement with the expected structures. As shown in Fig. S3, the polymerization was confirmed by the disappearance of the proton signals for the 2 and 5 positions (δ= 7.3 and 7.4 ppm) of the thiophene ring both for GO-f-PTAA and for GO-f-PTAA-co-PTh.
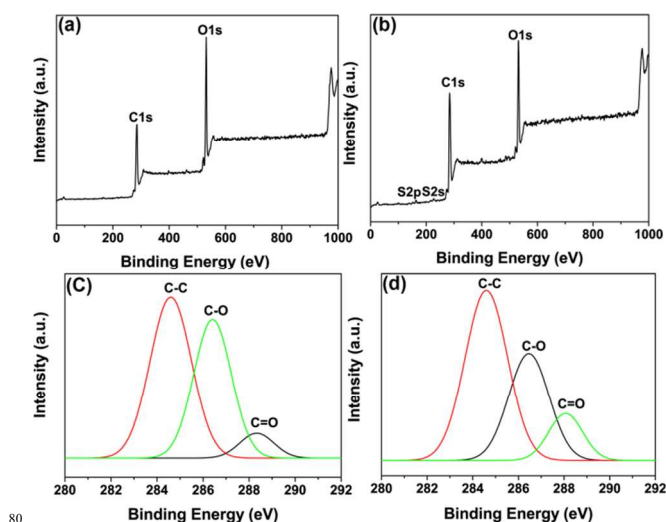
80 **Fig.1** X-ray photoelectron spectra of GO and GO-f-TAA: (a, b) wide scan spectra and (c, d) high resolution C 1s spectra.
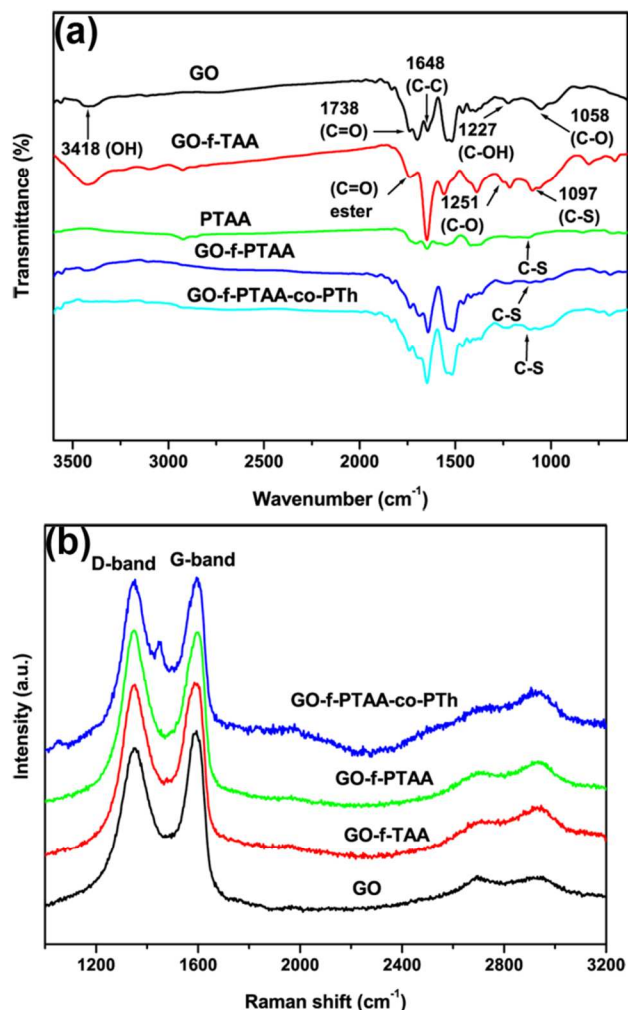
Fig. 2 (a) Fourier transform infrared spectra of GO, GO-f-TAA, PTAA, GO-f-PTAA and GO-f-PTAA-co-PTh and (b) Raman spectra of the GO, GO-f-TAA and GO-functionalized conducting polymers.

The thermal stability of GO, GO-f-PTAA, GO-f-PTAA-co-PTh, and pure PTAA was investigated using thermogravimetric analysis (Figs. S4a and S4b). The GO was thermally unstable and showed a sharp weight loss of 23.05 % between 120 to 220 °C, which was ascribed to the pyrolysis or decomposition of oxygen functional groups such as hydroxyl, carboxylic acid, and epoxide groups.[27] The TGA spectrum of pure PTAA indicated two-step thermal decomposition with (1) a weight loss from 300 to 370 °C due to decarboxylation and the loss of methylene groups and (2) a split of C-C and C-S bands of the ring around 460 °C.[28] From the TGA char residues, it is possible to estimate the polymer content in the composites. It was found that the degrees of polymer functionalization were around 7 and 14.8 wt% for GO-f-PTAA and GO-f-PTAA-co-PTh, respectively. Furthermore, the TGA curves showed that the thermal stability of the composites was increased. In particular, about 40% mass loss was reached around 439.2 °C for the pure PTAA, while the same mass loss did not occur until around 475.14 and 526.72 °C for the GO-f-PTAA and GO-f-PTAA-co-PTh composites, respectively, representing thermal stability increases of 35.94 °C and 87.52 °C. The increased thermal stability was attributed to the incorporation of

GO in the polymer matrix, which decreased the chain mobility of the polymer and hence increased its thermal stability.[29]

Fig. 3 displays TEM images of GO, GO-f-PTAA, and GO-f-PTAA-co-PTh. The TEM images of the GO sheets obtained after sonication in THF show wrinkled shapes, which is characteristic for single-layer or few-layer GO sheets. The GO-f-PTAA and GO-f-PTAA-co-PTh samples display individually dispersed monolayer or few-layer graphene sheets that are fully covered by the polymer. The overlaps and corrugation features of the nanocomposites occurred because of the high aspect ratio of the nanosheets. It can be seen that the edges of the polymer-functionalized GO sheets were much thicker than the pure GO sheets because of the coverage by polymers, which was also evidenced by the AFM images. Fig. S5 displays AFM images of GO and GO-f-PTAA-co-PTh. The average thickness of the GO sheets was found to be 1.38 nm, which is greater than the thickness of an ideal single-layer graphene sheet (0.34 nm) because of the presence of oxygen-containing groups such as carboxylic acid, hydroxyl, and epoxide groups in the GO sheets. However the GO-f-PTAA-co-PTh sheets are 3.459 nm thick because of the copolymer grafting. The increased thickness of the composites is due to the polymer functionalization of the GO sheets.
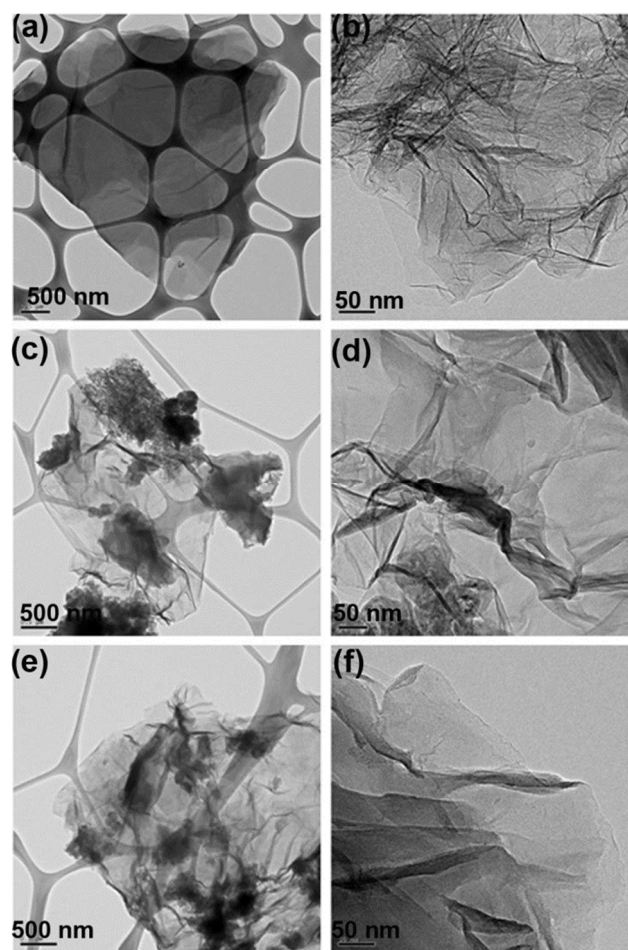
Fig. 3 Transmission electron microscopy images of (a, b) GO (c, d) GO-f-PTAA and (e, f) GO-f-PTAA-co-PTh composites.

To evaluate the compatibility of the covalently grafted graphene with the polymer, SEM images of spin-coated samples on silicon

wafers were observed. The GO-f-PTAA composites show a thickened layer structure with a rough surface due to the polymer functionalization (Fig. 4a). However in GO-f-PTAA-co-PTh samples, it seems that the graphene sheets are well dispersed in the polymer to yield a smooth morphology, suggesting that covalent functionalization results in dramatically improved dispersion of GO sheets (Fig. 4b). Furthermore, the chemical composition of the composites was analyzed by EDX spectroscopy, and the results revealed the presence of 5.38 and 7.43 % sulfur due to the presence of thiophene rings in the GO-f-PTAA and GO-f-PTAA-co-PTh composites, respectively (Figs. 4c and 4d).
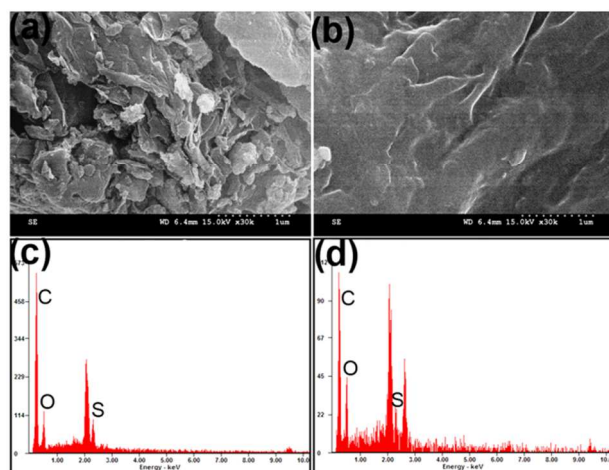

Fig. 4 Scanning electron microscopy image of (a) GO-f-PTAA and (b) GO-f-PTAA-co-PTh composites and EDX spectra of (c) GO-f-PTAA and (d) GO-f-PTAA-co-PTh.

Cyclic voltammetry measurements were carried out to demonstrate the potential applications of GO-f-PTAA and GO-f-PTAA-co-PTh composites in actuators, using 1 M H_2SO_4 with a potential range of -0.2 to 0.8 V versus Ag/AgCl at various scan rates (Fig. 5). A slightly distorted rectangular-type voltammogram was obtained for GO, indicating good charge propagation at the electrode. In addition, the GO shows a pair of oxidation and reduction peaks due to the transitional change of oxygen-containing functional groups between the quinone and hydroquinone states.[30] It can be seen that the cyclic voltammetry curve of pure PTAA shows redox behavior. However the covalent functionalization of PTAA with GO increases its electrochemical behavior, which is essential for achieving electrochemical actuation of conducting polymers.[31,32] Moreover, the unchanged rectangular voltammograms of the GO-f-PTAA-co-PTh sample even at a scan rate of 100 mV/s clearly signify the superior electrochemical behavior of the material at high scan rates. The electrical conductivity of compressed pellets from powder samples was measured using the four-probe measurement method. It was found that the pure PTAA did not show any conductivity value within the measured range, but the GO-f-PTAA and GO-f-PTAA-co-PTh composite samples showed conductivity values of 3.0×10^{-6} and 5.3×10^{-6} S/cm, respectively, indicating that there is an increase in the electrical conductivity due to functionalization with GO. In order to confirm the potential application of GO-functionalized conducting polymers as actuator materials, an air-operable conducting polymer

actuator was fabricated using the spin coating technique on cross-patterned aluminum electrodes, as shown in Fig. 6a. A cross-sectional SEM image of the GO-f-PTAA-co-PTh actuator is displayed in Fig. S6. It is believed that the covalent attachment of GO with the conducting polymer must improve its electrochemical properties and hence its actuation performance. Fig. 6b shows the bending displacement response of the GO-f-PTAA-co-PTh actuator for different electrolyte (LiTFSi) concentrations under an applied AC voltage of 3 V at constant frequency of 1 Hz. The bending displacement increased substantially as the LiTFSi concentration in the SPE was increased. This can be explained briefly as follows. When the voltage is applied by the cross-patterned electrode, positive and negative charges are generated separately on the GO-f-PTAA-co-PTh electrodes. Then, to maintain charge neutrality, the Li^+ ions move toward the negative charges and the $TFSi^-$ ions penetrate toward the positive charges, causing bending displacement of the actuator. As the concentration of the electrolyte was increased, more Li^+ and $TFSi^-$ ions penetrated into the GO-f-PTAA-co-PTh backbone, resulting in enhanced displacement of the actuator.[33,34] Moreover, the frequency of the displacement is consistent with the applied voltage, demonstrating air-operable actuation behavior of the composite material. In addition, the actuation performance of GO-f-PTAA-co-PTh was also investigated at different voltages (2, 3, and 4 V) with a constant frequency (1 Hz), and the results are displayed in Fig. 6c. As the voltage was increased, the bending displacement of the actuator increased (maximum strain of 0.78, 1.40, and 2.18 % at 2, 3, and 4 V, respectively). For comparative studies, we have also measured the actuation behavior of pure PTAA and GO-f-PTAA samples fabricated using methods similar to those used for the GO-f-PTAA-co-PTh composites. However, neither of these samples showed displacement under the applied voltages. This is due to the very low conductivity and poor electrochemical properties of pure PTAA, as shown in Fig. 5b. In the case of the GO-f-PTAA actuator, even though its electrochemical properties were improved after GO functionalization, it also exhibited no displacement in the actuation test because of its poor film forming capability during actuator fabrication due to the lower polymer content, as shown in the SEM images in Fig. 4a. In conclusion, only the GO-f-PTAA-co-PTh composite showed air-operable actuation behavior under an applied AC voltage.
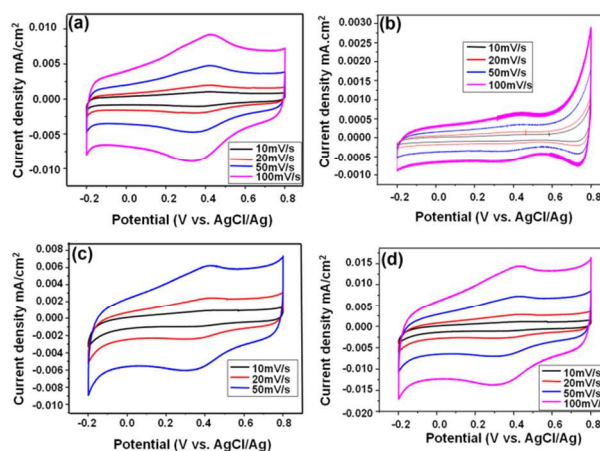
Fig. 5 Cyclic voltammograms of (a) GO, (b) PTAA, (c) GO-f-PTAA and (d) GO-f-PTAA-co-PTh composites.
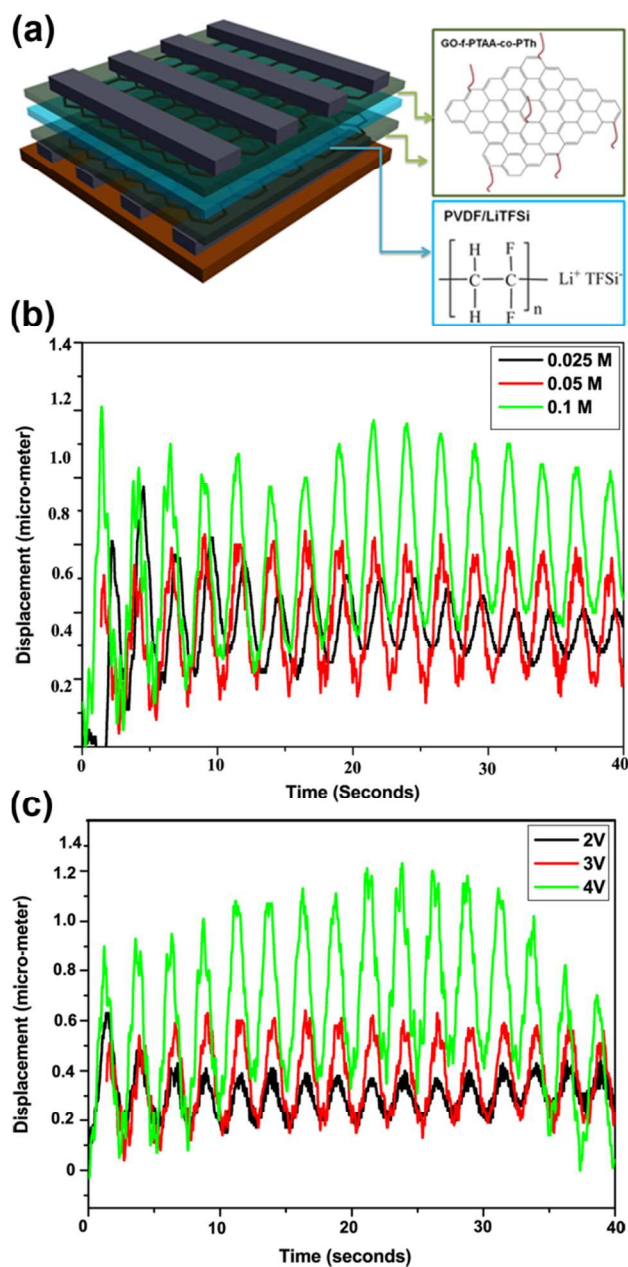
Fig. 6 (a) Air-operable actuator device structure, (b) actuator response for different electrolyte concentrations under an input AV voltage of 3V at a frequency of 1 Hz, and (c) actuation at different input voltages with a constant frequency of 1 Hz.

4 Conclusions

The GO was successfully covalently grafted with PTAA and its thiophene copolymer by a simple esterification reaction. The resultant composite materials were found to be processable in solvents such as DMF and THF and to exhibit substantially improved electrochemical properties. Using the processable GO-conducting polymer composites, we demonstrated the fabrication of an air-operable dry conducting polymer actuator using a cross-patterned electrode. The GO-f-PTAA-co-PTh composite showed air-operable actuation behavior under an applied AC voltage and has great potential for future implementation in the field of actuators.

Notes and references

aDepartment of Organic and Nano System Engineering, Konkuk University, Seoul 143-701, Republic of Korea. Fax: +82-2-457-8895; Tel: +82-2-450-3513; E-mail: jwcho@konkuk.ac.kr
bDepartment of Polymer & Fiber System Engineering, Chonnam National University, Gwangju 500-757, Republic of Korea
† Electronic Supplementary Information (ESI) available. See DOI: XXXXX

1. Y. B. Cohen, *Expert Rev. Med. Devices*, 2005, **2**, 731-740.
2. G. Kofod, *J. Phys. D: Appl. Phys.*, 2008, **41**, 215405-215416.
3. M. Karpelson, G. Y. Wei and R. J. Wood, *Sens. Actuators A.*, 2012, **176**, 78-89.
4. M. Hu, H. Du, S. F. Ling, Z. Zhou and Y. Li, *Mechatronics*, 2004, **14**, 153-161.
5. R. H. Baughman, *Synth. Met.*, 1996, **78**, 339-353.
6. E. Smela, *Adv. Mater.*, 2003, **15**, 481-494.
6. B. C. Achord and J. W. Rawlins, *Macromolecules*, 2009, **42**, 8634-8639.
7. Z. Bao and A. J. Lovinger, *Chem. Mater.*, 1999, **11,** 2607-2612.
8. C. O. Too, G. G. Wallace, A. K. Burrell, G. E. Collis, D. L. Officen, E. W. Boge, S. G. Brodie and E. J. Evans, *Synth. Met.*, 2001,**123**, 53-60.
9. M. Jeffries-EL, G. Sauve and R. D. McCullough, *Adv. Mater.*, 2004, **16**, 1017-1019.
10. B. Kim, L. Chen, J. Gong and Y. Osada, *Macromolecules*, 1999, **32**, 3964-3969.
11. P. Mukherjee, A. Dawn and A. K. Nandi, *Langmuir*, 2010, **26**, 11025-11034.
12. A. K. Geim and K. S. Novoselov, *Nat. Mater.*, 2007, **6**, 183-191.
13. S. K. Yadav, S. S. Mahapatra, J. W. Cho and J. Y. Lee, *J. Phys. Chem. C*, 2010, **114**, 11395-11400.
14. S. S. Mahapatra, S. K. Yadav, H. J. Yoo and J. W. Cho, *J. Mater. Chem.*, 2011, **21**, 7686-7691.
15. Z. Liu, Q. Liu, Y. Huang, Y. Ma, S. Yin, X. Zhang, W. Sun and Y. Chen, *Adv. Mater.*, 2008, **20**, 3924-3930.
16. F. Schwierz, *Nat. Nanotechnol.*, 2010, **5,** 487-496.
17. D. B. Velusamy, S. K. Hwang, R. H. Kim, G. Song, S. H. Cho, I. Bae and C. Park, , *J. Mater. Chem.*, 2012, **22,** 25183-25189.
18. J. Liang, Y. Xu, Y. Huang, L. Zhang, Y. Wang, Y. Ma, F. Li, T. Guo and Y. Chen, *J. Phys. Chem. C.*, 2009, **113**, 9921-9927.
19. Y. Lian, Y. Liu, T. Jiang, J. Shu, H. Lian and M. Cao, *J. Phys. Chem. C.*, 2010, **114**, 9659-9663.
20. H. J. Salavagione, M. A. Gomez and G. Martinez, *Macromolecules*, 2009, **42**, 6331-6334.
21. M. Giglioti, F. Trivinho-Strixino, J. T. Matsushima, L. O. S. Bulhoes and E. C. Pereira, *Sol. Energy Mater. Sol. Cells.*, 2004, **82**, 413-420.
22. D. Yang, A. Velamakanni, G. Bozoklu, S. Park, M. Stoller, R. D. Piner, S. Stankovich, I. Jung, D. A. Field, C. A. Ventrice Jr. and R. S. Rouff, *Carbon*, 2009, **47,** 145-152.
23. D. Yu, Y. Yang, M. Durstock, J. B. Baek and L. Dai, *ACS Nano*, 2010, **4**, 5633-5640.
24. N. A. Kumar, H. J. Choi, A. Bund, J. B. Baek and Y. T. Jeong, *J. Mater. Chem.*, 2012, **22**, 12268-12274.
25. A. C. Ferrari, J. C. Meyer, V. Scardaci, C. Casiraghi, M. Lazzeri, F. Mauri, S. Piscanec, D. Jiang, K. S. Novoselov, S. Roth and A. K. Geim, *Phys. Rev. Lett.*, 2006, **97**, 187401-187404.
26. Z. Tang, H. Kang, Z. Shen, B. Guo, L. Zhang and D. Jia, *Macromolecules*, 2012, **45,** 3444-3451.

27. S. Stankovich, D. A. Dikin, R. D. Piner, K. A. Kohlhaas, A. Kleinhammes, Y. Jia, Y. Wu, S. T. Nguyen and R. S. Ruoff, *Carbon,* 2007, **45,** 1558-1565.

28. C. Janaky, B. Endrodi, K. Kovacs, M. Timko, A. Sapi and C. Visy, *Synth. Met.,* 2010, **160,** 65-71.

29. V. H. Pham, T. V. Cuong, T. T. Dang, S. H. Hur, B. S. Kong, E. J. Kim, E. W. Shin and J. S. Chung, *J. Mater. Chem.,* 2011, **21,** 11312-11316.

30. M. D. Stoller, S. Park, Y. Zhu, J. An and R. S. Ruoff, *Nano Lett.,* 2008, **8**, 3498-3502.

31. L. Jianhua, A. Junwei, Z. Yecheng, M. Yuxiao, L. Mengliu, Y. Mei and L. Songmei, ACS Appl. Mater. Interfaces, 2012, 4, 2870−287.

32. N. A. Kumar, H. J. Choi, A. Bund, J.- B. Baek and Y. T. Jeong, J. Mater. Chem., 2012, 22, 12268−12274.

33. S. Hara, T. Zama, W. Takashima and K. Kaneto, *J. Mater. Chem.*, 2004, **14**, 1516-1517.

34. B. Gaihre, G. Alici, G. M. Spinks and J. M. Cairney, *Sens. Actuators B.*, 2011, **155**, 810-816.